

Quantum decoherence in the rotation of small molecules

A. Adelswärd and S. Wallentowitz*

Emmy–Noether Nachwuchsgruppe “Kollektive Quantenmessung und Rückkopplung an Atomen und Molekülen”, Fachbereich Physik, Universität Rostock, Universitätsplatz 3, D-18051 Rostock, Germany

Abstract. The dynamics of non-polar diatomic molecules interacting with a far-detuned narrow-band laser field, that only may drive rotational transitions, is studied. The rotation of the molecule is considered both classically and quantum mechanically, providing links to features known from the heavy symmetric top. In particular, quantum decoherence in the molecular rotation, being induced by spontaneous Raman processes, is addressed. It is shown how this decoherence modifies the rotational dynamics in phase space.

PACS numbers: 33.80.-b, 03.65.Yz, 42.50.Ct

1. Introduction

Molecules interacting with electromagnetic fields foster a variety of dynamical phenomena. Specific wave packets of the internuclear vibration have been excited by shaped fs laser pulses [1]. Such vibrational quantum states have then been reconstructed by molecular emission tomography [2, 3]. Furthermore, control of the internal molecular quantum state could be achieved [4–8], for eventually enhancing chemical reactions.

Besides these applications of pulsed fields, also interactions with cw laser fields or static fields reveal interesting effects. For instance, the axis of paramagnetic molecules can be aligned in pendular states by applying magnetic fields [9, 10]. Furthermore, it has been shown how electric fields align polar molecules [11]. Non-polar molecules, on the other hand, seem to be rather isolated from the influence of electric fields. They are infrared inactive and thus their rotation is essentially undamped and isolated from the electromagnetic vacuum. Clearly this does not hold for the internuclear vibration and, in addition, the rotational statistics determines via ro-vibrational coupling its relaxation and decoherence properties [12, 13].

Nevertheless, a permanent dipole moment being absent, non-polar molecules still can be polarised by electrical fields and thus feel an effective alignment force when an anisotropic polarisability prevails. The quantum-mechanical eigenstates and energies have been discussed in Ref. [14], where it has been shown that the dependence of the eigenenergies on the field intensity can be used for providing a dipole trapping force. Recent experiments have implemented such a dipole trap for molecules [15].

In general the topic of producing [16–21], cooling [22, 23], and trapping of ultra-cold molecules [15, 24] became a major focus of research in recent years. Given the ultra-low temperatures of a condensed atomic or possibly molecular gas, the molecular rotation, representing the lowest energy scale apart from centre-of-mass motion, then should play an important role. For sufficiently cold molecules one might expect decoherence first to appear

* email: sascha.wallentowitz@physik.uni-rostock.de

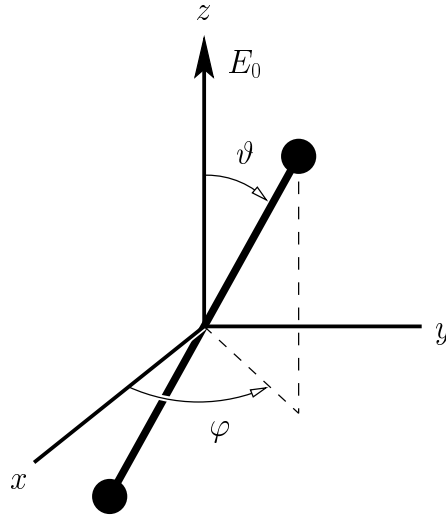


Figure 1. Diatomic molecule in an electric field pointing in z direction. The angles ϑ and φ specify the orientation of the molecular axis with respect to the laboratory frame.

on the rotational energy scale before affecting the energetically higher degrees of freedom, such as the internuclear vibration. Moreover, the molecular rotation provides a toolbox for implementing various textbook examples of mechanics, such as spherical pendula and the motion of rigid bodies.

In particular, we will focus here on homonuclear, diatomic molecules in a far-detuned linear-polarised laser field. This is a setup relevant also for trapping of photo-associated ultra-cold molecules in a dipole trap [15]. In Sec. 2 a brief review is given on the classical description of the motion of the molecular axis. A link to a quantum description in terms of stimulated two-photon Raman processes is then presented in Sec. 3. Moreover, the theory is extended there by including spontaneous Raman processes in form of a quantum master equation. The effects due to these spontaneous processes on the molecular rotation are evaluated in Sec. 4 where we provide a phase-space picture by using a Wigner function for the molecular rotation.

2. Classical mechanical analogue

2.1. Classical dynamics

Consider a diatomic molecule in an electric field of amplitude E_0 pointing towards the z direction. The potential energy in such a field is given by

$$V(\vartheta) = -dE_0 \cos \vartheta - \frac{1}{2}E_0^2 \Delta\alpha \cos^2 \vartheta, \quad (1)$$

where d is the permanent dipole moment of the molecule and $\Delta\alpha = \alpha_{\parallel} - \alpha_{\perp}$ denotes the anisotropy of the polarisability with respect to fields parallel and perpendicular to the molecular axis. The direction of this axis with respect to the electric field is specified by the enclosing angle ϑ , cf. Fig. 1.

The molecular axis specifies the z' -axis of a body-fixed coordinate system, whose orientation with respect to the laboratory frame is specified by Euler angles. From the

Lagrange equations one obtains the equations of motion for these as

$$\Theta(\ddot{\vartheta} - \dot{\varphi}^2 \sin \vartheta \cos \vartheta) + \frac{\partial V(\vartheta)}{\partial \vartheta} = 0, \quad (2)$$

$$\dot{\varphi} \sin^2 \vartheta = \text{const}, \quad (3)$$

where Θ is the moment of inertia perpendicular to the molecular axis. Moreover, the conservation of energy E reads

$$\Theta(\dot{\vartheta}^2 + \dot{\varphi}^2 \sin^2 \vartheta) = 2[E - V(\vartheta)]. \quad (4)$$

Note that for our case the relevant Euler angles ϑ and φ coincide with the spherical angles as depicted in Fig. 1.

The angular-momentum \mathbf{L} can be expressed in the laboratory frame by the angles and their time derivatives as

$$\mathbf{L} = \Theta \begin{pmatrix} \dot{\vartheta} \cos \varphi - \dot{\varphi} \sin \vartheta \cos \vartheta \sin \varphi \\ \dot{\vartheta} \sin \varphi + \dot{\varphi} \sin \vartheta \cos \vartheta \cos \varphi \\ \dot{\varphi} \sin^2 \vartheta \end{pmatrix}. \quad (5)$$

From Eqs (3) and (5) it is seen that the component of the angular momentum in direction of the applied field is a constant of motion: $L_z = \text{const}$. Thus the tip of the angular-momentum moves in a plane normal to the electric-field direction. Using the constant of motion L_z , Eq. (4) can be rewritten as

$$\frac{\Theta \dot{\vartheta}^2}{2} = E - U(\vartheta), \quad (6)$$

where the new potential reveals a centrifugal-type barrier

$$U(\vartheta) = \frac{T_z}{\sin^2 \vartheta} - U_d \cos \vartheta - U_\alpha \cos^2 \vartheta. \quad (7)$$

For later purposes we have introduced here the potential depths $U_d = dE_0$, $U_\alpha = \Delta\alpha E_0^2/2$ and the z -part of the kinetic energy $T_z = L_z^2/(2\Theta)$.

A molecule with permanent dipole moment, $d \neq 0$, omitting its anisotropic polarisability, $\alpha_{\parallel} \approx \alpha_{\perp}$, reveals a potential of a spherical pendulum, as shown in Fig. 2. The motion in φ with constant angular momentum L_z is superimposed by a nutation in ϑ , which is equivalently described by a heavy symmetrical top with vanishing moment of inertia along the (molecular) body axis. The harmonically approximated nutation frequency is in this case $\omega = \sqrt{U_d/\Theta}$.

However, for the case of non-polar ($d = 0$) but polarisable molecules ($\alpha_{\parallel} > \alpha_{\perp}$), which is the focus of this paper, the anisotropic polarisability produces a $\cos^2 \vartheta$ potential, cf. Fig. 3, which for $L_z \neq 0$ cannot be cast into the form of a spherical pendulum. Nevertheless, a spherical-pendulum-type motion can be expected, since also for this case the solution $\vartheta(t)$ can be obtained in terms of elliptic integrals. Expressed in terms of Jacobian elliptic functions [25] it reads,

$$\cos \vartheta(t) = \frac{\cos \vartheta_0 \text{cn}(\omega t, m) - \sqrt{(\cos^2 \vartheta_0 - c_l)(c_u - \cos^2 \vartheta_0)} m/c_u \text{sn}(\omega t, m) \text{dn}(\omega t, m)}{1 - (c_u - \cos^2 \vartheta_0) \text{sn}^2(\omega t, m) m/c_u}, \quad (8)$$

where ϑ_0 is the initial angle at time $t = 0$. The constants appearing in Eq. (8) are given as

$$m = \frac{1}{\epsilon + 1}, \quad (9)$$

$$c_{l,u} = \frac{m - \frac{1}{2}}{m} \mp \sqrt{\frac{1}{4m^2} - \kappa_z}, \quad (10)$$

$$\omega = \sqrt{\frac{2U_\alpha c_u}{\Theta m}}, \quad (11)$$

where the scaled energies $\epsilon = E/U_\alpha$ and $\kappa_z = T_z/U_\alpha$ have been used.

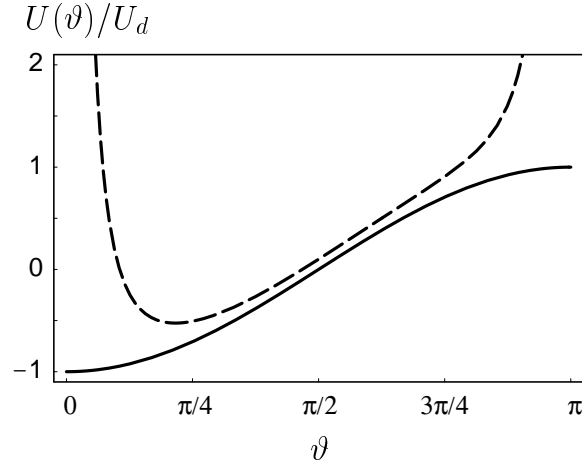


Figure 2. Nutation potential $U(\vartheta)$ for a polar molecule scaled by the potential depth U_d . Solid (dashed) curve corresponds to $T_z/U_d=0$ (0.1).

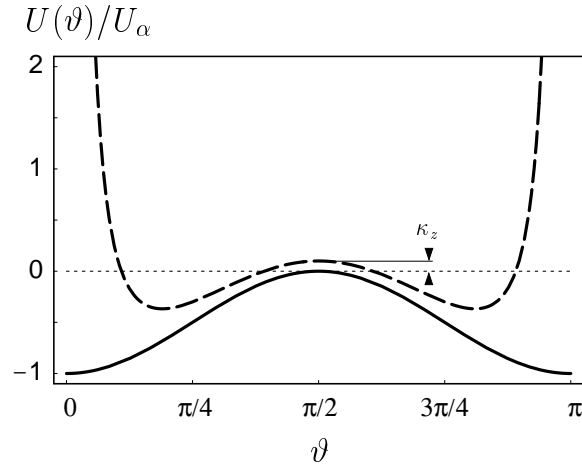


Figure 3. Nutation potential $U(\vartheta)$ for a nonpolar, polarisable molecule scaled by U_α . Solid (dashed) curve corresponds to $\kappa_z = T_z/U_\alpha = 0$ (0.1).

2.2. Classical types of motion

In the asymptotic limit of large energies $\epsilon \gg 1$, $\text{sn}, \text{cn} \rightarrow \sin, \text{cos}$ and $\text{dn} \rightarrow 1$ so that $\cos \vartheta(t) = \cos(\vartheta_0 + \omega t)$ results, which corresponds to the free rotator case with angular velocity $\omega \rightarrow \sqrt{2E/\Theta}$. In this limit all three vector components of the angular momentum are conserved quantities.

For lower energies the potential barriers lead to modifications, supporting several types of motion. For $\kappa_z = 0$ unbound motion occurs for $\epsilon > 0$ where the amplitude of the oscillation of ϑ attains the full π range, see solid curve in Fig. 4. Given an initial angular momentum only in x direction, the molecular axis then continuously rotates around the x axis so that while L_x is modulated due to the potential barriers, it does not change its sign, see solid curve in Fig. 5.

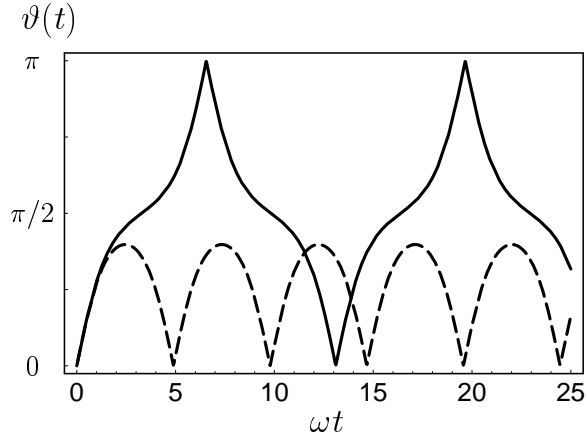


Figure 4. Nutation angle ϑ over scaled time ωt for $\kappa_z = 0$, $\vartheta_0 = 0$, $L_y(0) = 0$ and $2\Theta U_\alpha/\hbar^2 = 0.025$. Scaled energies and x -components of angular momentum are: $\epsilon = 0.024$, $L_x(0)/\hbar = 0.16$ (solid curve); $\epsilon = -0.1$, $L_x(0)/\hbar = 0.15$ (dashed curve).

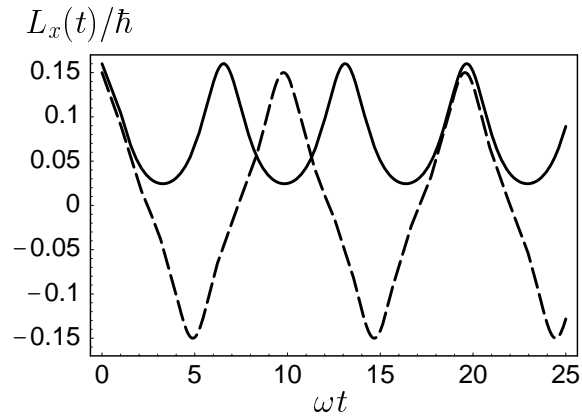


Figure 5. L_x/\hbar over scaled time ωt for the same parameters as in Fig. 4.

On the other hand, for the same case of $\kappa_z = 0$, for energies $\epsilon < 0$ the angle ϑ is subject to a reflection at the light-induced potential barrier. Thus the range of ϑ values is restricted, as seen for the dashed line in Fig. 4. In addition, since $\dot{\vartheta}$ changes its sign at the reflecting barrier, the angular momentum L_x correspondingly crosses zero and thus rotations with positive and negative orientations subsequently interchange, cf. dashed line in Fig. 5. Note that for $\kappa_z > 0$ the motion of ϑ is additionally bound by reflections at the centrifugal barriers near $\vartheta = 0$ and π .

3. Quantum dynamics of the molecular rotation

3.1. Implementation via two-photon Raman transitions

For implementing the dynamics described so far, not only static electric fields can be used. Also linear polarised cw optical fields, that are far detuned from electronic resonances, have

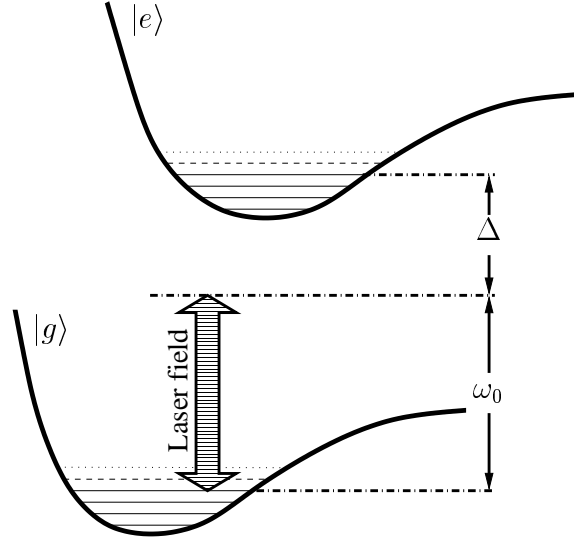


Figure 6. Excitation scheme for implementing rotational Raman transitions.

been shown to produce a similar interaction [14]. In this way one can take advantage of large polarisabilities of non-polar molecules to attain deep potential wells for the nutation angle. The specific excitation scheme for a dimer, depicting only the two lowest electronic potential surfaces that provide a $^1\Sigma \leftrightarrow ^1\Sigma$ dipole transition, is shown in Fig. 6.

In order to avoid resonant vibronic transitions and to be left with the sought two-photon processes, a sufficiently large detuning Δ from the bare electronic resonance frequency is required. Given an optical field of spectral width much smaller than vibrational frequencies ω_ν , stimulated Raman transitions occur that only affect the rotational degree of freedom. However, the relative rate of spontaneous vs stimulated Raman transitions, Γ/Δ , with Γ being the bare electronic linewidth of the dipole transition, shows that even for large detuning, $\Delta \gg \Gamma$, a certain number of spontaneous processes occur. These processes not only lead to an incoherent effect on the molecular rotation, such as relaxation and quantum decoherence, but also excite the internuclear vibration via Franck–Condon transitions.

Nevertheless, as long as the laser remains detuned from resonant vibronic transitions, the electronic and vibrational degrees of freedom can be eliminated to obtain equations of motion for the molecular rotation alone. This is achieved by consistently eliminating the electronic coherences and electronic excited-state populations, keeping only terms up to second order in the molecule-light interaction. In Franck–Condon approximation the vibrational degree of freedom can then be traced over [26]. The requirement of avoiding resonant vibronic transitions leads to a maximum interaction time on which the molecule stays vibrationally sufficiently cold, which can be estimated as

$$t \ll \Delta^2 / (\eta^2 \Gamma \omega_\nu \Omega_R). \quad (12)$$

Here $\Omega_R = |d_{ge} E_0|^2 / (4\hbar^2 \Delta)$ is the Raman Rabi frequency with d_{ge} being the electric-dipole matrix element between electronic ground and excited states. The linear polarised electric field is specified by $E(t) = \hat{n}_z E_0 \cos(\omega_0 t)$ with ω_0 being an optical frequency far-detuned from vibronic resonance and \hat{n}_z being the unit vector in z direction. Using these parameters the light-induced potential depth results as $U_\alpha = \hbar \Omega_R$.

The parameter η is the ratio of the difference of internuclear equilibrium distances in ground and excited electronic states to the spatial extent of the vibrational ground-state wave packet. Since $\eta < 10$ for alkali dimers, in the weak-field regime [$\Omega_R < \hbar/(2\Theta)$] this time corresponds to a very large number of free rotational periods.

Under these conditions the equations of motion for the orientation of the molecular axis in the far detuned optical field can be cast into a master equation of Lindblad form [26]:

$$\dot{\hat{\sigma}} = -\frac{i}{\hbar}[\hat{T} + \hat{V}, \hat{\sigma}] + \sum_{i=x,y,z} \left(\hat{S}_i \hat{\sigma} \hat{S}_i^\dagger - \frac{1}{2} \hat{S}_i^\dagger \hat{S}_i \hat{\sigma} - \frac{1}{2} \hat{\sigma} \hat{S}_i^\dagger \hat{S}_i \right). \quad (13)$$

Here $\hat{\sigma}$ is the reduced rotational density operator of the molecule and the free kinetic energy is given by [27]

$$\hat{T} = \hat{\mathbf{J}}^2 / (2\Theta). \quad (14)$$

The stimulated rotational Raman transitions then provide the sought potential in the form

$$\hat{V} = -\hbar\Omega_R \hat{n}_z^2, \quad (15)$$

where in terms of spherical angles the unit-vector operator \hat{n}_z reads $\langle \vartheta, \varphi | \hat{n}_z = \cos \vartheta | \langle \vartheta, \varphi |$, so that

$$\langle \vartheta, \varphi | \hat{V} = -U_\alpha \cos^2(\vartheta) | \langle \vartheta, \varphi | \quad (16)$$

recovers the potential as discussed for the classical treatment.

The spontaneous rotational Raman transitions are given in terms of the operators \hat{S}_i , with $i = x, y, z$ denoting the polarisation of the spontaneously emitted photon. They read

$$\hat{S}_i = \sqrt{\frac{\Gamma\Omega_R}{\Delta}} \hat{n}_i \hat{n}_z, \quad (17)$$

with \hat{n}_i ($i = x, y, z$) being unit vectors pointing into the corresponding directions. In the representation of spherical angles these jump operators can be cast in vector form to:

$$\langle \vartheta, \varphi | \hat{S} = \sqrt{\frac{\Gamma\Omega_R}{\Delta}} \begin{bmatrix} \cos \varphi \sin \vartheta \cos \vartheta \\ \sin \varphi \sin \vartheta \cos \vartheta \\ \cos^2 \vartheta \end{bmatrix} | \langle \vartheta, \varphi |. \quad (18)$$

3.2. Stimulated Raman processes

For vanishing bare electronic linewidth, $\Gamma = 0$, a unitary evolution is recovered from the master equation (13) that can be reformulated in terms of the Schrödinger equation

$$i\hbar \partial_t |\Psi\rangle = (\hat{T} + \hat{V}) |\Psi\rangle, \quad (19)$$

with the Hamiltonian given by Eqs (14) and (15). In the $|\vartheta, \varphi\rangle$ representation the evolution of the wavefunction $\Psi(\vartheta, \varphi) = \langle \vartheta, \varphi | \Psi\rangle$ reads

$$i\hbar \dot{\Psi}(\vartheta, \varphi) = - \left\{ \frac{\hbar^2}{2\Theta} \left[\frac{1}{\sin \vartheta} \partial_\vartheta (\sin \vartheta \partial_\vartheta) + \frac{1}{\sin^2 \vartheta} \partial_\varphi^2 \right] + U_\alpha \cos^2 \vartheta \right\} \Psi(\vartheta, \varphi). \quad (20)$$

Using the ansatz $\Psi(\vartheta, \varphi) = S_{lm}(z) \exp(im\varphi)$, with $\hbar m = J_z$ being a constant of motion, and $z = \cos \vartheta$, the energy eigenstates are obtained from the angular oblate spheroidal wave equation [25]

$$\left\{ \frac{\hbar^2}{2\Theta} \left[\partial_z [(1-z^2)\partial_z] - \frac{m^2}{1-z^2} \right] + U_\alpha z^2 + E_{lm} \right\} S_{lm}(z) = 0. \quad (21)$$

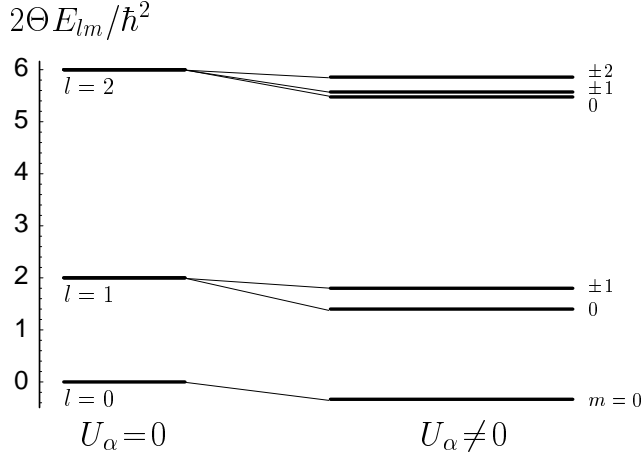


Figure 7. Change of energy eigenvalues due to the light interaction for the value $2\Theta U_\alpha/\hbar^2 = 1$.

The corresponding eigenenergies E_{lm} can be expanded in powers of the interaction potential U_α as

$$E_{lm} = \frac{\hbar^2}{2\Theta} l(l+1) - \frac{U_\alpha}{2} \left[1 + \frac{1-4m^2}{(2l-1)(2l+3)} \right] + \dots \quad (22)$$

They manifest a partial removal of the degeneracy with respect to m , as shown in Fig. 7. The properties of these eigenstates and their angular confinement have been discussed in detail in Ref. [11].

The quantum dynamics of a system prepared quite analogously as discussed for the classical treatment, i.e. with an initial average angular momentum pointing only in x direction, is shown in Fig. 8. Here an initial coherent angular-momentum state [28] of the form

$$|j, \alpha, \beta\rangle = \sum_{m=-j}^j \sqrt{\binom{2j}{j+m}} [\sin(\alpha/2)]^{j+m} [\cos(\alpha/2)]^{j-m} e^{-i(j+m)\beta} |jm\rangle, \quad (23)$$

for $j = 2$, $\alpha = \pi/2$, and $\beta = 0$ has been used. Classically that would correspond to the case $\kappa_z = 0$ where reflections in the motion of ϑ can only occur due to the light-induced potential. But from Eq. (23) it is clear that we deal with an initial state containing states $|j, m\rangle$ with all possible values for m :

$$|\Psi_1\rangle = |j=2, \alpha=\pi/2, \beta=0\rangle \\ = \frac{1}{4} |2, -2\rangle + \frac{1}{2} |2, -1\rangle + \sqrt{\frac{3}{8}} |2, 0\rangle + \frac{1}{2} |2, 1\rangle + \frac{1}{4} |2, 2\rangle. \quad (24)$$

Thus part of the wave packet in ϑ will also be reflected by centrifugal barriers.

In Fig. 8 an oscillation of $\langle \hat{J}_x \rangle$ between positive and negative values is observed that is characteristic for reflections of the wavefunction at potential barriers. However, the transient behaviour at the crossing of zero indicates that part of the wave packet in ϑ is transmitted through the barrier, and that reflected and transmitted parts interfere for the short time where they spatially overlap.

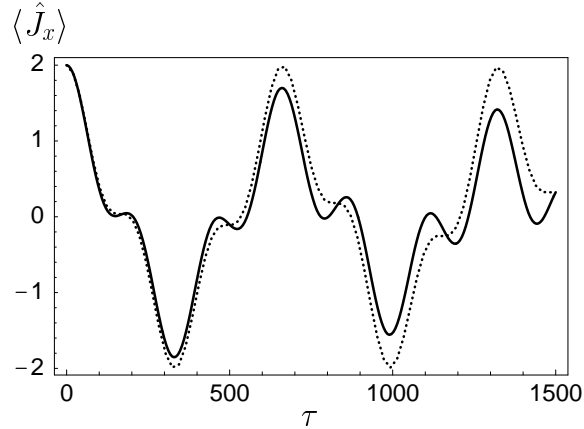


Figure 8. Dynamics of $\langle \hat{J}_x(t) \rangle$ over scaled, dimensionless time $\tau = t\hbar/(2\Theta)$. The laser interaction strength is $\hbar\Omega_R/(2\Theta) = 0.1$ and the detuning $\Gamma/\Delta = 0.01$ (solid line). The dotted line corresponds to $\Gamma = 0$.

3.3. Spontaneous processes

When spontaneous processes are included in the dynamics, i.e for $\Gamma > 0$, the full master equation (13) must be solved. Due to the scaling of complexity of this numerical problem with the number of required rotational levels, it is advantageous to employ a quantum trajectory method. Then individual realisations of state vectors can be calculated and finally an ensemble average over the set of realisation reproduces the sought density matrix.

Individual trajectories are comprised of non-unitary evolutions with the effective Hamiltonian

$$\hat{H}_{\text{eff}} = \hat{T} + \hat{V} \left(1 + \frac{i\Gamma}{2\Delta} \right), \quad (25)$$

describing the conditioned evolution when no spontaneous processes occur, intermitted by spontaneous Raman processes described by the application of the jump operators \hat{S}_i . As can be seen from their definition (18), these operators may excite the motion in the angle φ , by producing via \hat{S}_x and \hat{S}_y a weighting of the corresponding probability amplitude $\Psi(\vartheta, \varphi)$ in φ . Thus motion in φ and consequently the angular momentum component \hat{J}_z are getting excited by spontaneous Raman processes.

This can be observed in Fig. 9, where the variance of \hat{J}_z is plotted over time. For $\Gamma > 0$ a monotonous increase of the variance is observed, indicating that the kinetic energy is subject to heating. Of course the spontaneous Raman scattering will also lead to a suppression of coherent processes and the oscillations of the average angular momentum will be damped, cf. solid curve in Fig. 8.

4. Decohering dynamics in phase space

4.1. Spherical Wigner functions

In the same way as the angular-momentum coherent states are a generalisation of the familiar harmonic-oscillator coherent states, also the concept of phase-space quasi-probability distributions can be defined on the angular-momentum phase space [29]. Here we employ a

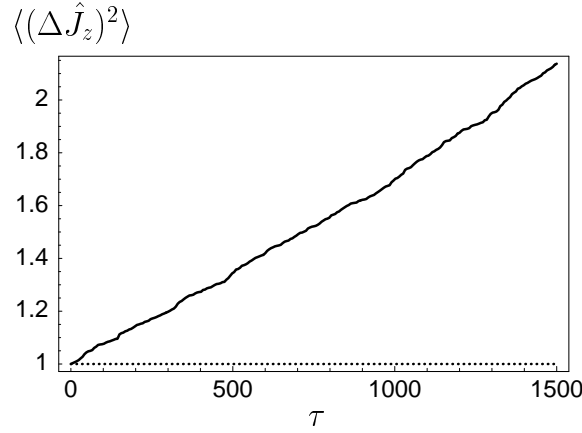


Figure 9. Variance of \hat{J}_z over scaled, dimensionless time, $\tau = t\hbar/(2\Theta)$. The parameters are the same as in Fig. 8.

Wigner function, which in the $(2j+1)$ -dimensional Hilbert space of angular momentum j , is defined in terms of the density operator $\hat{\sigma}$ and the spherical harmonics, $Y_{sm}(\theta, \varphi)$, as defined in Refs [30,31]

$$W_j(\vartheta, \varphi) = \sqrt{\frac{2j+1}{4\pi}} \sum_{s=0}^{2j} \sum_{m=-s}^s Y_{sm}(\vartheta, \varphi) \text{Tr}(\hat{T}_{j,sm}^\dagger \hat{\sigma}). \quad (26)$$

The multipole operators are defined by

$$\hat{T}_{j,sm} = \sqrt{2s+1} \sum_{m'm''} (-1)^{j-m'} \begin{pmatrix} j & s & j \\ -m' & m & m'' \end{pmatrix} |jm'\rangle \langle jm''|, \quad (27)$$

with $\begin{pmatrix} j_1 & j_2 & j_3 \\ m_1 & m_2 & m_3 \end{pmatrix}$ being the Wigner 3j symbol. The factor in front of Eq. (26) ensures normalisation to unity.

As the laser interaction will result in a change of the rotational quantum number j of the molecule we consider a sum of Wigner functions over all possible values of j :

$$W(\vartheta, \varphi) = \sum_{j=0}^{\infty} W_j(\vartheta, \varphi). \quad (28)$$

Albeit the sum over j , this phase-space distribution is not a complete description of the rotational quantum state. However, it proves useful for illustrating the laser-induced dynamics. For alternative approaches defining phase-space distributions independent of the particular value of j , see Refs [32–34]. Moreover, it should be noted that even though the angular-momentum coherent states are analogous to the harmonic-oscillator ones in many respects, the Wigner function of angular-momentum coherent states is weakly negative. This negativity decreases with increasing value for j and reaches zero only in the (classical) limit $j \rightarrow \infty$.

4.2. Time evolution of the Wigner function

Figure 10 shows the time evolution of the system starting initially from the state $|\Psi_1\rangle$, cf. Eq. (24). The phase-space distribution is shown for a scaled time $\tau = t\hbar/(2\Theta) = 660$ after the first full period of oscillation of $\langle \hat{J}_x \rangle$ (upper left plot), and then at later times in steps

of quarter periods. One can see that the system almost returns to its initial coherent state after one period, when the spontaneous emission is neglected (left column). The peak in phase space has then returned to its initial position at $\vartheta = \pi/2$ and $\varphi = 0$. In the course of time the peak splits and after a half period, at $\tau = 990$, two peaks appear at $\vartheta = \pi/2$, $\varphi = 0, \pi$. That corresponds to an average angular momentum pointing now in negative x direction. Note that between half and full cycles, at $\tau = 830$ and $\tau = 1165$, the phase-space distribution develops several smaller peaks and also negative regions of the Wigner function appear. Including the spontaneous Raman processes, the structures in phase-space generally are smoothed and negativities are suppressed. This can be seen from the right column of plots in Fig. 10.

As another example, in Fig. 11 a superposition of two coherent angular-momentum states,

$$|\Psi_2\rangle = \sqrt{\frac{2}{5}} \left(|j=2, \alpha=\pi/2, \beta=\pi/4\rangle + |j=2, \alpha=\pi/2, \beta=-\pi/4\rangle \right), \quad (29)$$

has been taken as the initial quantum state. This state has a strong negative region of the Wigner function centred at $\vartheta = \pi/2$, $\varphi = 0$. The plots of the Wigner function for this initial state show the same oscillatory behaviour as Fig. 10, with the negative peak being shifted to $\varphi = 0, \pi$ at half periods.

However, comparing the time evolution of these two cases one can see that the difference between the unitary and non-unitary evolution is much more pronounced in the case of the coherent state. Especially at the times between completed half and full cycles (at $\tau = 830$ and $\tau = 1165$), when also the Wigner function of the time-evolved coherent state shows relative strong negative regions, one observes that these negativities have become weaker in the presence of spontaneous emission. The populations in the j -level manifolds for the final interaction time of Figs 10 and 11 are shown in Fig. 12. It can be seen that for both the coherent state and the superposition of coherent states the populations in $j = 0, 4$ have increased by a few percent at the expense of the population in the initial manifold $j = 2$.

That the coherent state in this example actually is much more sensitive to decoherence may seem counter-intuitive at first sight, but one should keep in mind that the angular-momentum coherent state is not classical in the usual sense of a harmonic-oscillator coherent state. That is, as has been seen above its Wigner function in general is not positive everywhere. Furthermore, angular-momentum coherent states apparently are not in general the most robust states against decoherence, as are harmonic oscillator coherent states for linearly coupled reservoirs.

The substantial difference in how these two cases are affected by decoherence due to spontaneous processes can also be observed in Fig. 13, where the time evolution of the purity of the density operator is shown. It can be seen that the superposition state (29) develops much slower into a mixed state compared to the coherent state.

The type of decoherence mechanism is in general determined by the form of the operators \hat{S}_i , see Eqs (17) and (18). In our case these operators differ from raising and lowering operators $\hat{J}_\pm = \hat{J}_x \pm i\hat{J}_y$, and thus our decoherence mechanism itself is different from that discussed in Refs [35, 36], though for special choices of initial conditions particular features may be similar.

5. Summary and conclusions

We have considered a diatomic homonuclear molecule in a far-detuned, linear-polarised light field. First the classical motion of the molecule was studied. For the case of a molecule

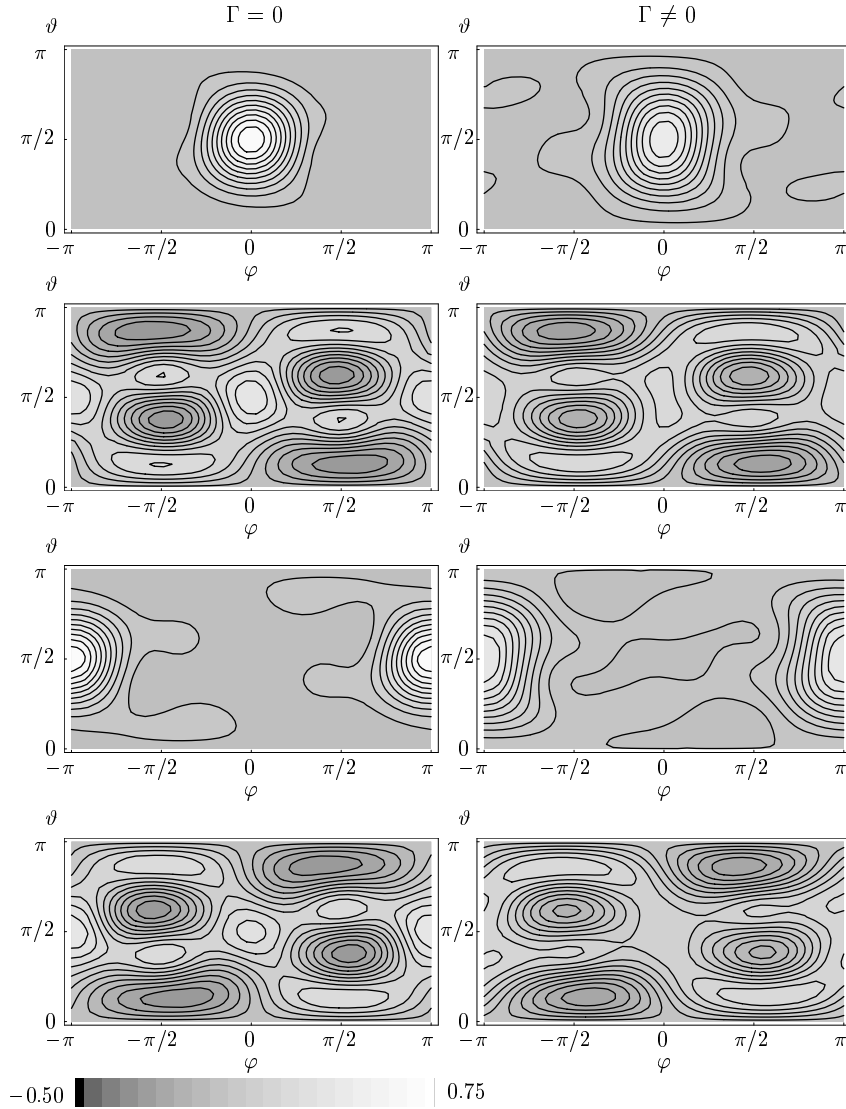


Figure 10. Time evolution of the coherent state $|\Psi_1\rangle$. From top to bottom the figures show the Wigner function at scaled times $\tau = 660$, $\tau = 830$, $\tau = 990$, and $\tau = 1165$. Parameters are the same as in Fig. 8 and $\tau = t\hbar/(2\Theta)$.

with a permanent dipole, the potential was seen to be that of a spherical pendulum. For non-polar molecules, however, the potential is of a different form, but the solution for the nutation angle still could be found in terms of elliptic integrals. The motion was then treated quantum mechanically, where stimulated and spontaneous Raman processes were taken into account by a master equation. Solving this equation both for an angular-momentum coherent state and a superposition state, the effects of the decoherence induced by the spontaneous processes were compared. It was seen that, in this particular example, the superposition state was more robust to decoherence than the coherent state.

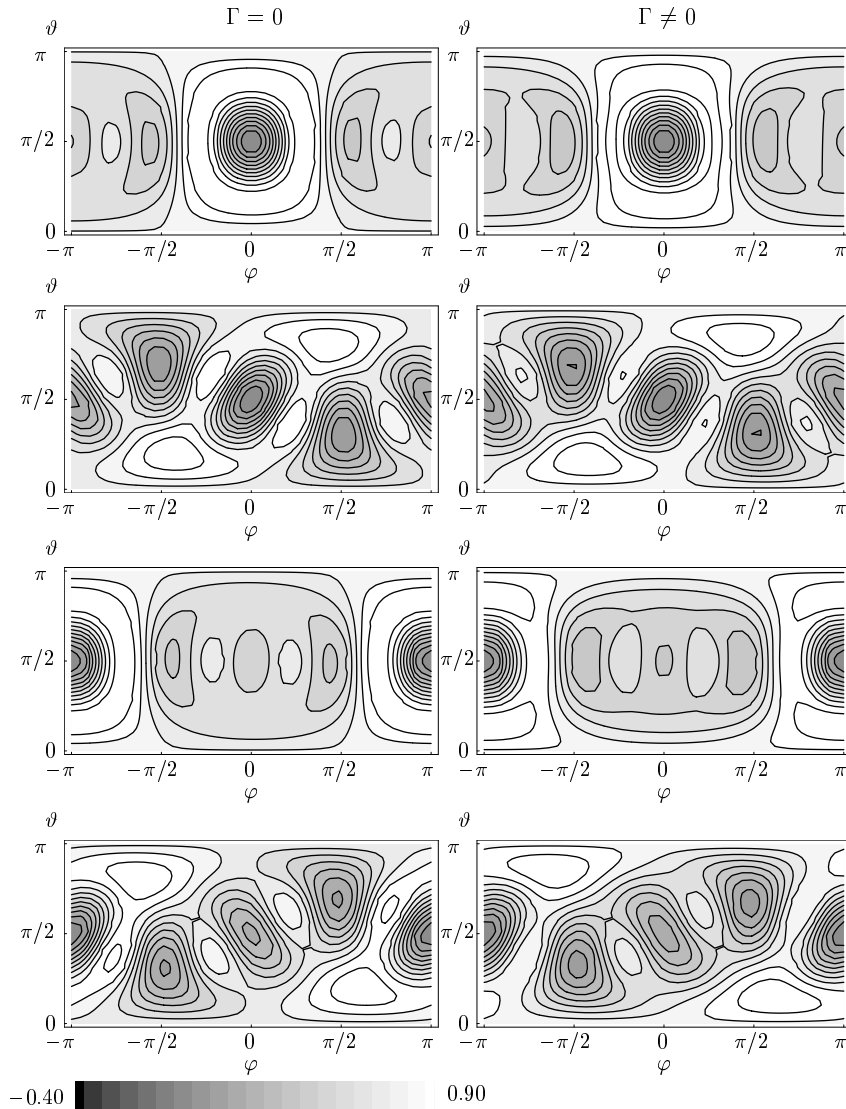


Figure 11. Time evolution of the initial superposition state $|\Psi_2\rangle$. Parameters are the same as in Fig. 10 and $\tau = t\hbar/(2\Theta)$.

Acknowledgements

This research was supported by Deutsche Forschungsgemeinschaft.

References

- [1] Kohler B, Yakovlev V V, Che J, Krause J, Messina M, Wilson K R, Schwenter N, Whitnell R M and Yan Y J 1995 *Phys. Rev. Lett.* **74** 3360
- [2] Dunn T J, Walmsley I A and Mukamel S 1995 *Phys. Rev. Lett.* **74** 884
- [3] Walmsley I A and Waxer L 1998 *J. Phys. B* **31** 1825

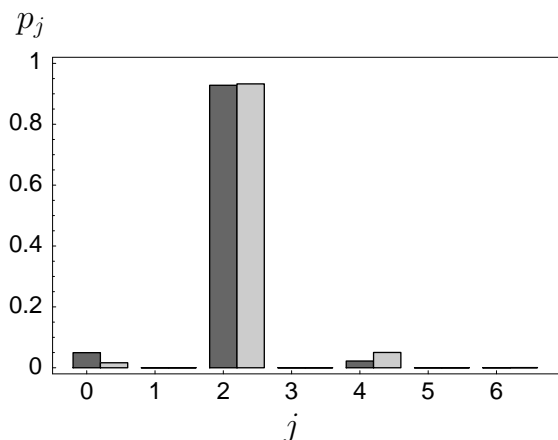


Figure 12. Populations p_j at the interaction time $\tau = 1165$ for the coherent angular-momentum state (light bars) and the superposition of coherent angular-momentum states (dark bars). Parameters are the same as for Figs 10, 11.

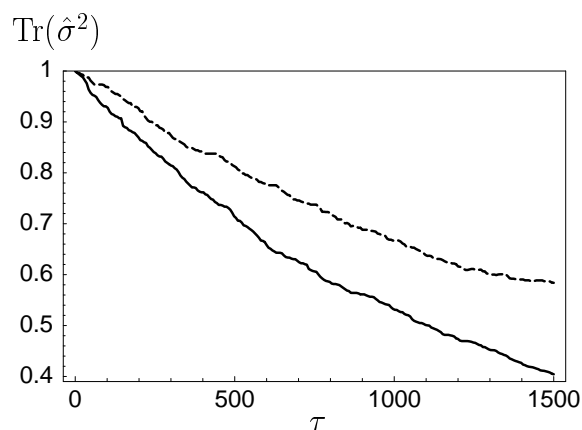


Figure 13. Purity for the initial coherent state (solid curve) and initial superposition state (dashed curve). Parameters are the same as in Fig. 8 and $\tau = t\hbar/(2\Theta)$.

- [4] Judson R S and Rabitz H 1992 *Phys. Rev. Lett.* **68** 1500
- [5] Rabitz H, de Vivie-Riedle R, Motzkus M and Kompa K 2000 *Science* **288** 824
- [6] Bardeen C J, Yakovlev V V, Wilson K R, Carpenter S D, Weber P M and Warren W S 1997 *Chem. Phys. Lett.* **280** 151
- [7] Assion A, Baumert T, Bergt M, Brixner T, Kiefer B, Seyfried V, Strehle M and Gerber G 1998 *Science* **282** 919
- [8] Pearson B J, White J L, Weinacht T C and Bucksbaum P H 2001 *Phys. Rev. A* **63** 063412
- [9] Friedrich B and Herschbach D R 1992 *Z. Phys. D* **24** 25
- [10] Slenczka A, Friedrich B and Herschbach D R 1994 *Phys. Rev. Lett.* **72** 1806
- [11] Rost J M, Griffin J C, Friedrich B and Herschbach D R 1992 *Phys. Rev. Lett.* **68** 1299
- [12] Brif C, Rabitz H, Wallentowitz S and Walmsley I A 2001 *Phys. Rev. A* **63** 063404
- [13] Wallentowitz S, Walmsley I A, Waxer L J and Richter Th 2002 *J. Phys. B* **35** 1967
- [14] Friedrich B and Herschbach D R 1995 *Phys. Rev. Lett.* **74** 4623
- [15] Takekoshi T, Patterson B M and Knize R J 1998 *Phys. Rev. Lett.* **81** 5105

- [16] Fioretti A, Comparat D, Crubellier D, Dulieu O, Masnou-Seeuws F and Pillet P 1998 *Phys. Rev. Lett.* **80** 4402
- [17] Nikolov A N, Eyler E E, Wang X T, Li J, Wang H, Stwalley W C and Gould P L 1999 *Phys. Rev. Lett.* **82** 703
- [18] Wynar R, Freeland R S, Han D J, Ryu C and Heinzen D J 2000 *Science* **287** 1016
- [19] Gerton J M, Strekalov D, Prodan I and Hulet R G 2000 *Nature* (London) **408** 692
- [20] Shaffer J P, Chalupcak W and Bigelow N P 2001 *Phys. Rev. A* **63** 021401(R)
- [21] McKenzie C, Hecker Denschlag J, Häffner H, Browaeys A, de Araujo L E E, Fatemi F K, Jones K M, Simsarian J E, Cho D, Simoni A, Tiesinga E, Julienne P S, Helmerson K, Lett P D, Rolston S L and Phillips W D 2002 *Phys. Rev. Lett.* **88** 120403
- [22] Weinstein J D, deCarvalho R, Guillet T, Friedrich B and Doyle J M 1998 *Nature* **395** 148
- [23] Bethlem H L, Crompvoets F M H, Jongma R T, van de Meerakker S Y T and Meijer G 2002 *Phys. Rev. A* **65** 053416
- [24] Vanhaecke N, de Souza Melo W, Laburthe Tolra B, Comparat D and Pillet P 2003 *Phys. Rev. Lett.* **89** 063001
- [25] Abramowitz M and Stegun I A 1972 *Handbook of mathematical functions* (Dover Publications, 9th ed): For Jacobian elliptic functions see chap. 16, p. 567, for oblate spheroidal wave equations see Eq. 21.6.4, p. 753.
- [26] Adelswärd A, Wallentowitz S and Vogel W 2003 *Phys. Rev. A* **67** 063805
- [27] For notational correctness we use in the quantum case the angular momentum operator $\hat{\mathbf{J}}$ instead of $\hat{\mathbf{L}}$.
- [28] Arecchi F T, Courtens E, Gilmore R and Thomas H 1972 *Phys. Rev. A* **6** 2221
- [29] Agarwal G S 1981 *Phys. Rev. A* **24** 2889
- [30] Dowling J P, Agarwal G S and Schleich W P 1994 *Phys. Rev. A* **49** 4101
- [31] Benedict M G and Czirják A 1999 *Phys. Rev. A* **60** 4034
- [32] Földi P, Benedict M G and Czirják A 1998 *Acta Phys. Slov.* **48** 335
- [33] Brif C and Mann A 1999 *Phys. Rev. A* **59** 971
- [34] Chumakov S M, Klimov A B and Wolf K B 2000 *Phys. Rev. A* **61**, 034101
- [35] Braun D, Braun P A and Haake F 2000 *Opt. Commun.* **179** 411
- [36] Földi P, Czirják A and Benedict M G 2001 *Phys. Rev. A* **63** 033807